Thermal conductance of epitaxial interfaces

Ruxandra M. Costescu,* Marcel A. Wall, and David G. Cahill†
Department of Materials Science and Engineering, Coordinated Science Laboratory, and Seitz Materials Research Laboratory, University of Illinois, Urbana, Illinois 61801

(Received 23 December 2002; published 27 February 2003)

The thermal conductance of interfaces between epitaxial TiN and single crystal oxides is measured at temperatures between 79.4 and 294 K using time-domain thermoreflectance. The analysis method relies on the ratio of the in-phase and out-of-phase signals of the lock-in amplifier for more accurate data analysis. The validity of this approach is tested by measurements on 6.5, 11.8, and 25 nm thick thermally oxidized SiO_2 on Si. The thermal conductances G of TiN/MgO(001), TiN/MgO(111), and TiN/Al_2O_3(0001) interfaces are essentially identical and in good agreement with the predictions of lattice dynamics models and the diffuse mismatch model with a four-atom fcc unit cell. Near room temperature, $G \approx 700$ M W m^{-2} K^{-1}, ≈ 5 times larger than the highest values reported previously for any individual interface.

DOI: 10.1103/PhysRevB.67.054302 PACS number(s): 68.60.Dv, 68.35.−p

I. INTRODUCTION

The thermal conductance of interfaces plays a critical role in the transport of thermal energy in nanometer-scale devices,[1] composites,[2] semiconductor superlattices,[3] thin film multilayers,[4] and nanocrystalline materials.[5] The acoustic-mismatch and diffuse-mismatch models predict this conductance based on assumptions about the behavior of phonons at the interface. In the acoustic-mismatch model, phonon transmission and reflection are calculated from the mass density and anisotropic elastic constants of materials; at short wavelengths, the calculations must take into consideration the dynamics of the lattice.[6] The diffuse-mismatch model, on the other hand, assumes that phonons are randomly and elastically scattered at the interface; the transmission coefficient is given by the ratio of the densities of vibrational states on either side of the interface.[7]

Although these models have greatly advanced understanding of thermal transport across interfaces, theory and experiment[7–9] are often in poor agreement at elevated temperatures where the full spectrum of vibrational modes is thermally excited. The cause of this disagreement is not known. In addition, the scope of the experimental literature is limited and experimentalists have not yet observed the high or low extremes of conductance predicted by theory[9,10] and have not isolated contributions to heat transport at interfaces by anharmonicity, electron-phonon coupling,[11] interface disorder,[12] or altered interface bonding.[13] To enhance understanding of solid-solid interface thermal conductance, we have measured thermal transport through highly perfect interfaces between epitaxial TiN and single crystal oxides. Our data closely approach the theoretical predictions and we thereby demonstrate the utility of these models for predicting interface conductance near room temperature.

II. EXPERIMENTAL DETAILS

A. Sample preparation and characterization

Single crystal substrates MgO(001), MgO(111), and Al_2O_3(0001), are annealed in air at 1400 °C for 4 h to remove polishing damage. Atomic-force microscopy is used to characterize the morphology of the crystal surfaces. The surface morphologies consist of atomically flat terraces (≈ 1 μm wide for MgO and ≈ 400 nm wide for Al_2O_3) separated by single-height and multiple-height atomic steps; the step-densities reflect the small miscut of the crystals, $\theta < 0.1°$.

We grow amorphous SiO_2 oxide layers on Si by furnace annealing: the 6.5 and 11.8 nm SiO_2 films were grown by thermal oxidation of commercial Si wafers in a clean-room furnace at UIUC; the 25 nm SiO_2 layer was grown in the microelectronics lab at UC Berkeley. The thickness of the SiO_2 layers is measured by variable-angle spectroscopic ellipsometry. We use x-ray reflectivity measurements to confirm that TiN deposition does not change the oxide thickness.

Volatile contaminants of the SiO_2/Si and oxide-crystal surfaces are removed by heating the substrates in the UHV deposition chamber for an hour at 850 °C. Titanium nitride layers are then deposited by reactive magnetron sputtering at 850 °C.[14] TiN is a refractory material with low electrical resistivity $\rho = 12.4$ $\mu\Omega$ cm and a metallic gold appearance. At $\lambda = 770$ nm, the complex index of refraction of TiN is $\tilde{n} = 0.55 + 3.8i$. The thermoreflectance dR/dT of TiN at $\lambda \approx 800$ nm is unusually large; measurements of the optical constants by spectroscopic ellipsometry at 300 and 700 K give $dR/dT \approx 1.6 \times 10^{-4}$ K^{-1}.

The thickness of TiN films is chosen to be ≈ 4 times the optical absorption depth, $\alpha^{-1} = \lambda/(4\pi k) = 16$ nm. The thickness of TiN deposited on SiO_2 is measured by picosecond acoustics using an averaged longitudinal speed of sound of 10.3 nm ps^{-1}. Due to the small acoustic mismatch of TiN and MgO or Al_2O_3, acoustic echoes are not visible. Instead, we use electrical sheet resistance and x-ray reflectivity to determine the TiN film thickness on MgO and Al_2O_3 substrates.

X-ray diffraction is used to characterize the texture of the TiN films. TiN films deposited on amorphous SiO_2 under our conditions are polycrystalline and do not show a preferred orientation. TiN deposited on MgO(001) is epitaxial and forms essentially single-crystal TiN(001).[14] (TiN and MgO have the same NaCl crystal structure and almost identical

 ©2003 The American Physical Society

lattice constants.) On MgO(111) and $Al_2O_3(0001)$, TiN(111) is aligned epitaxially but with approximately equal populations of the two possible variants of the cubic stacking sequence.

B. Time-domain thermoreflectance

We apply the time-domain thermoreflectance (TDTR) method introduced by Paddock and Eesley[15] and Young and co-workers[16] but modify the analysis to take advantage of the extra information in the out-of-phase signal of the lock-in amplifier.[17] Our TDTR measurements use a mode-locked Ti:sapphire laser that produces a series of <0.5 ps pulses at a rate of 80.6 MHz. The laser output is split into a "pump" beam and a "probe" beam whose relative optical path lengths are adjusted via a mechanical delay stage. The optical design includes a single microscope objective that focuses the beams, collimates the reflected probe beam and forms a dark-field microscopy image of the surface of the sample on a CCD camera.[17,18] Samples are mounted in a LN_2 cryostat. We use pump and probe beam powers of 6 and 9 mW, wavelength $\lambda = 770$ nm, and a $1/e^2$ beam radius of $\approx 8\ \mu$m. For TiN, 15% of the energy in each pump pulse heats the TiN film by ≈ 0.5 K at room temperature and ≈ 3 K at 80 K. For the worst case, Al_2O_3 substrates at room temperature, the steady-state heating of the film surface is ≈ 2 K.

III. DATA ANALYSIS AND THERMAL MODELING

In a modulated pump-probe experiment, the differences in reflected probe intensity caused by the pump pulse appear at the modulation frequency of the pump beam and are extracted with lock-in detection. Interpretation of the lock-in signal as a function of modulation frequency f and delay time t between pump and probe is not straightforward.[19] The lock-in signal has an in-phase and out-of-phase component $V(t) = V_{in}(t) + iV_{out}(t)$. Typically, only $V_{in}(t)$ is considered in the analysis but the additional information in the out-of-phase signal[17,19] provides a simple method of correcting for nonidealities in the experiment: both V_{in} and V_{out} are changed by the same factor by defocusing of the pump beam and changes in the pump-probe overlap and therefore $V_{in}(t)/V_{out}(t)$ is a more robust measurement than V_{in} alone. For example, intentionally degrading the spatial overlap of the pump and probe beams to an extent that reduces the lock-in signals by 50% typically results in $<5\%$ change in $V_{in}(t)/V_{out}(t)$.

To interpret $V_{in}(t)/V_{out}(t)$, we begin with a calculation of the frequency domain temperature response $\Delta\mathcal{T}(\nu)$ of one-dimensional heat flow in a multilayer sample using matrix methods.[20] Convolution in the frequency domain gives

$$S(q) = \Delta\mathcal{T}(q/\tau + f) + \Delta\mathcal{T}(q/\tau - f),$$

$$D(q) = \Delta\mathcal{T}(q/\tau + f) - \Delta\mathcal{T}(q/\tau - f),$$

$$\frac{V_{in}(t)}{iV_{out}(t)} = \frac{\sum_{q=-\infty}^{\infty} S(q)\exp(i2\pi tq/\tau)}{\sum_{q=-\infty}^{\infty} D(q)\exp(i2\pi tq/\tau)}, \tag{1}$$

where τ is the time between laser pulses. We determine the thermal conductivity of a thin layer or the thermal conductance of an interface by comparing the measured $V_{in}(t)/V_{out}(t)$ to Eq. (1) and optimizing the free parameters. Since the thermal diffusion time across the 16 nm optical absorption depth of the TiN layer is <5 ps, for $t > 50$ ps, we can safely assume that the temperature is homogeneous through the optical absorption depth of the metal film; and therefore, $\Delta R = (dR/dT)\Delta T$, where ΔR is the reflectivity change, dR/dT is the thermoreflectance of TiN, and ΔT is the temperature excursion at the surface of the sample.

Lateral heat flow in the thin TiN layer is negligible but radial heat flow in the substrate can produce a significant correction to the one-dimensional heat flow calculation, particularly at low temperatures when the thermal diffusivity D_s of the substrate is large. The main effect of the radial heat flow in the substrate is to reduce V_{out} by a small factor; V_{out} is mostly controlled by the imaginary part of frequency response at the modulation frequency $\Delta\mathcal{T}(f)$. To include a first order correction for radial heat flow in our analysis, we rotate the complex phase of the substrate contribution to $\Delta\mathcal{T}(f)$ by the factor $\exp[iD_s/(w_0^2\pi f)]$. For our experimental parameters at room temperature, this factor is always small: with $f \approx 9.8$ MHz and $D_s \approx 1\ \mathrm{cm^{-2}\ s^{-1}}$ (appropriate for Si), the correction to V_{out} is $\approx 5\%$. With MgO and Al_2O_3 substrates, the correction for radial heat flow is $<1\%$ at room temperature.

At low temperatures, however, the corrections due to radial heat flow become significant and we must abandon a strict reliance on Eq. (1). In this low temperature regime, we adjust the effusivity of the substrate in the model to fit $V_{in}(t)/V_{out}(t)$ at short delay times $t \approx 100$ ps. This approach does not alter the determination of thin film thermal conductivity or interface thermal conductance: at low temperatures the temperature drop in the substrate makes only a small contribution to the total thermal response.

The thermal model needed to analyze a three-layer (TiN film, interface layer, substrate) experiment contains up to seven parameters: the thickness h, specific heat C, and thermal conductivity Λ of the TiN and interface layers, and the effusivity of the substrate. But because the thermal conductivity of the TiN film is high and the TiN film thickness is large compared to the thickness of the interface layer, the model is sensitive to only three combinations of these parameters: the total heat capacity per unit area $h_{TiN}C_{TiN}$, the thermal conductance of the interface layer $G = \Lambda_{SiO_2}/h_{SiO_2}$, and the effusivity of the substrate $\Lambda_s C_s$. We use literature values for the heat capacities, Refs. 21–24 for Si, TiN, SiO_2, and MgO, Al_2O_3, respectively. We use our previous measurements of the substrate thermal conductivities: Ref. 25 for Si and Ref. 26 for MgO and Al_2O_3. The thermal conductivity

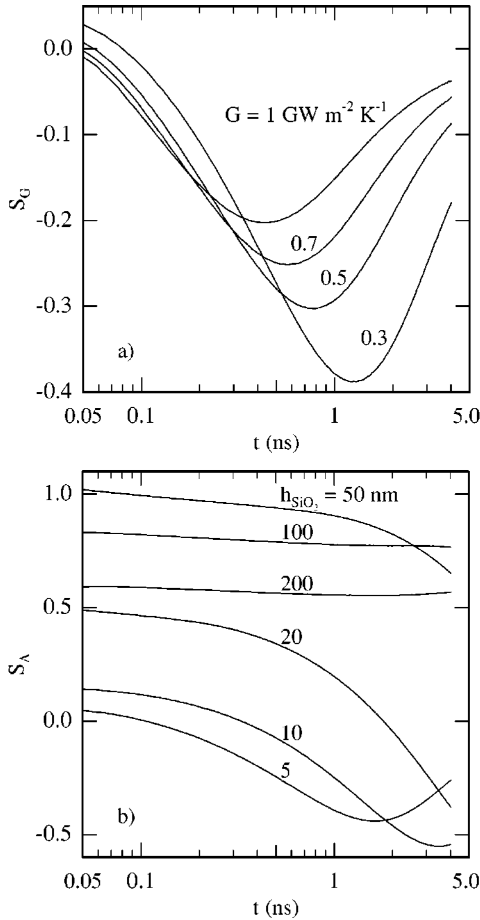

FIG. 1. Sensitivity parameters [Eq. (2)] as a function of delay time. (a) Sensitivity S_G to the thermal conductance G of the interface for 53 nm TiN/MgO(111); the curves are labeled by the thermal conductance of the interface. (b) Sensitivity S_Λ to the thermal conductivity Λ of the thin SiO_2 layer in a 57 nm TiN/SiO_2/Si sample; the curves are labeled by the thickness of the SiO_2 layer.

of TiN is given by the Wiedemann-Franz-Lorenz law and measurements of the electrical resistivity.[14]

To evaluate the sensitivity of our experiments to the material properties we wish to measure, we calculate the logarithmic derivatives of $V_{\text{in}}(t)/V_{\text{out}}(t)$ with respect to the thermal conductance of the interface G or, for a thin film sample, with respect to the thermal conductivity of the film Λ:

$$S_G=\frac{\partial \ln\left[-\frac{V_{\text{in}}(t)}{V_{\text{out}}(t)}\right]}{\partial \ln G}$$

$$S_\Lambda=\frac{\partial \ln\left[-\frac{V_{\text{in}}(t)}{V_{\text{out}}(t)}\right]}{\partial \ln \Lambda}. \tag{2}$$

These parameters S have a complicated dependence on the thermal properties and delay time t, see Fig. 1, but we note a few important features: (i) for an interface with a large thermal conductance, $S_G<0$ and the minimum becomes deeper and moves to larger t with decreasing G; (ii) for a thin film sample, S_Λ continues this trend with increasing film thickness; (iii) for thicker layers, $S_\Lambda>0$, S_Λ becomes independent of t, and has a maximum value for a film thickness of ≈ 50 nm.

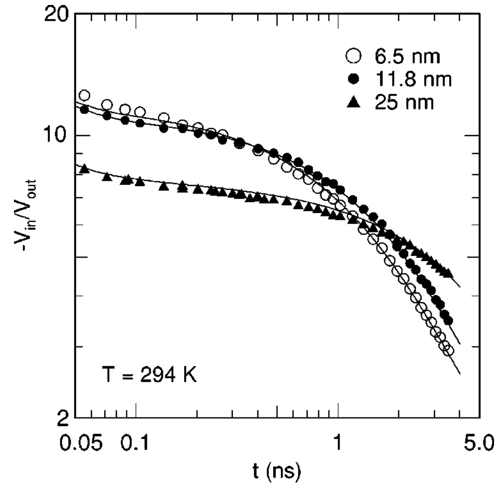

FIG. 2. Time-domain thermoreflectance (TDTR) data acquired at room temperature for TiN/SiO_2/Si samples. Data points are labeled by the SiO_2 thickness. The ratio of the in-phase to out-of-phase signals at the 9.8 MHz modulation frequency is plotted as a function of the delay time t between pump and probe. The solid lines are fits based on Eq. (1) with the thermal conductivity of SiO_2 as the one free parameter.

IV. RESULTS AND DISCUSSION

A. Thermal conductivity of thin SiO_2

To verify our methods and demonstrate the utility of our approach for thermal transport measurements for thin films, we prepared three samples of ≈ 60 nm thick TiN films on 6.5, 11.8, and 25.0 nm SiO_2 layers on Si substrates. This structure was chosen because the thermal properties of Si and SiO_2 are well known; and because previous work[4] has shown that the thermal conductivity of thick layers of thermally grown SiO_2 are essentially identical to the bulk. TDTR data for these three samples and theoretical fits for room temperature are shown in Fig. 2.

The thermal conductivities of the thin SiO_2 layers are plotted as a function of temperature in Fig. 3. The fitting was based on the simplest possible model, with three components: the TiN film, the SiO_2 layer, and the Si substrate; the interface thermal resistances are included in the thermal resistance of the SiO_2 layer. Data for the 25 nm thick layer are in excellent agreement with measurements for bulk[27] SiO_2. Data for the 11.8 and 6.5 nm samples are lower. The reduction in apparent thermal conductivity for the thinner SiO_2 layers is expected for these ultrathin oxides, due to the thermal resistance of the Si/SiO_2 and TiN/SiO_2 interfaces. Therefore, we conclude that the use of $V_{\text{in}}(t)/V_{\text{out}}(t)$ in the analysis of TDTR data provides an accurate method for determining the thermal conductance $G=\Lambda/h$ of a thin layer.

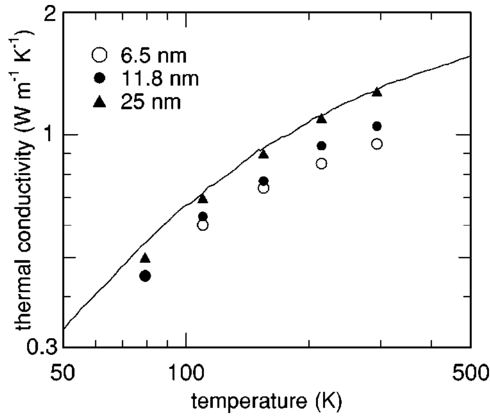

FIG. 3. Thermal conductivity of SiO_2 layers in $TiN/SiO_2/Si$; data points are labeled by the SiO_2 thickness. The bulk thermal conductivity of SiO_2 is shown for comparison (Ref. 27, solid line).

B. Thermal conductance of TiN/MgO and TiN/Al_2O_3 interfaces

We next turn our attention to the thermal conductance of epitaxial TiN interfaces. We can expect that TiN/MgO(001) interfaces are structurally more perfect than typical metal/ceramic interfaces and essentially free of misfit dislocations and stacking faults. TiN/MgO(111) contains a high density of stacking faults at the interface but few misfit dislocations because the lattice mismatch between TiN and MgO is small. Since the oxygen-oxygen nearest neighbor spacing in the basal plane of α-Al_2O_3 ($d=0.275$ nm) is $\approx 8\%$ smaller than the N-N spacing in TiN(111), $TiN/Al_2O_3(0001)$ should contain large densities of both stacking faults and misfit dislocations.

Example TDTR data and fits are shown in Fig. 4 for TiN/MgO(111) at three temperatures. Values for G extracted from the fits to the data are plotted as Fig. 5. Our data for G of TiN epitaxial interfaces are a factor of >5 higher than previous studies[8,9] of metal/Al_2O_3 interfaces at $T>80$ K. Part of this difference can be attributed to the higher frequencies of vibrational modes in TiN; e.g., the averaged longitudinal speed of sound[28] in TiN is 10.3 nm ps^{-1}, a factor of ≈ 1.6 larger than Al. But we attribute the bulk of the difference to greater perfection of the materials; in other words, we believe the data shown in Fig. 5 represent the intrinsic transport properties of the interfaces, free from the effects of phonon or electron scattering by defects in the near-interface regions of the substrate and film.[7] Our data also approach the high values of interface thermal conductance that have been observed in molecular dynamics simulations of Si grain boundaries.[10]

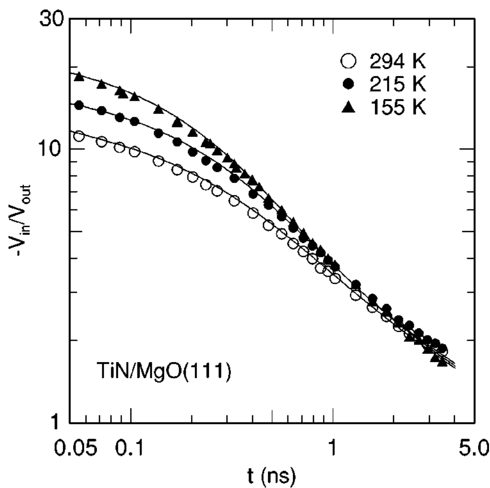

FIG. 4. Time-domain thermoreflectance data for thermal transport across an epitaxial TiN/MgO(111) interface; data points are labeled by the measurement temperature. The ratio of the in-phase to out-of-phase signals of the lock-in amplifier is plotted as a function of the delay time t. The solid lines are fits based on Eq. (1) with the interface conductance G as the one free parameter.

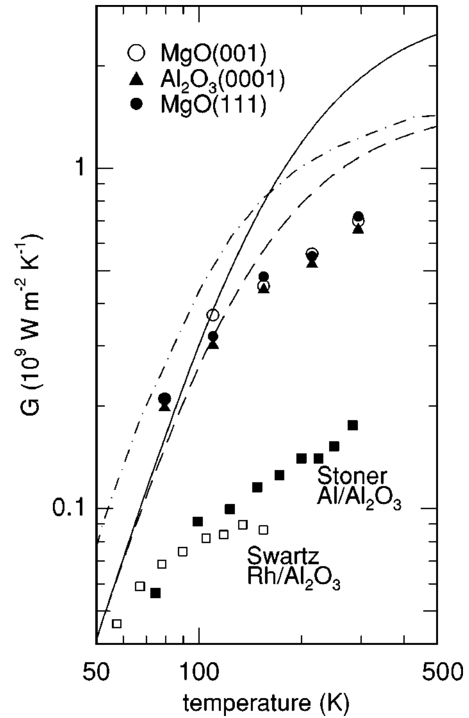

FIG. 5. Thermal conductance of epitaxial TiN/MgO(001), $TiN/Al_2O_3(0001)$, and TiN/MgO(111) interfaces as a function of temperature. The solid line is the DMM prediction for TiN/MgO, the dashed line is the DMM prediction excluding optical modes, and the dashed-and-dotted line is the LD calculation of Ref. 6 for $K'=M'=2$ scaled by $a=0.21$ nm and a Debye temperature of 740 K. Data for the conductance of Al/Al_2O_3, Ref. 9 (filled squares), and Rh/Al_2O_3, Ref. 8 (open squares) are for comparison.

We compare our experimental results to the predictions of the diffuse-mismatch model (DMM) and lattice dynamics (LD) calculations, see Fig. 5. For DMM calculations,[7] we use a Debye model to describe the phonon densities of states in TiN and MgO. (Sound velocities for TiN and MgO are from Refs. 28 and 29.) TiN, MgO, and Al_2O_3 have similar Debye temperatures so the transmission coefficient for phonons in the DMM model is $\approx 1/2$. The DMM prediction is ≈ 2 G W m^{-2} K^{-1} at room temperature, much larger than the data. Since the optical modes of TiN and MgO have small group velocities and therefore do not transport heat as efficiently as the acoustic modes, we also consider a DMM calculation that eliminates 1/2 of the vibrational modes by

treating each TiN or MgO molecule as a single unit. The agreement with the data improves to better than 30%.

The predictions of LD calculations for a model fcc-fcc interface[6] (also using four atoms per conventional fcc unit cell) give almost identical results near room temperature because the increase in the transport created by the larger phonon transmission coefficient[6] is compensated by the decrease in thermal transport produced by mode dispersion. Since the acoustic mismatch between TiN and MgO or TiN and Al_2O_3 is small, the transmission coefficient for phonons is nearly unity. At low temperatures, $T < 150$ K, the prediction of the LD model is a factor of 2 larger than the DMM, reflecting the factor of 2 difference in transmission coefficients.

Surprisingly, we do not observe significant differences in G for the three TiN interfaces. In particular, the 8% in-plane lattice mismatch between TiN(111) and Al_2O_3(0001)—and the interface stacking faults in the TiN/MgO(111) and TiN/Al_2O_3 samples—do not modify the thermal transport significantly. Apparently, the additional interface disorder in these samples does not change the phonon transmission coefficient significantly. Therefore, we are left with two possible interpretations of these experimental results: (i) the interface disorder in all samples produces strong phonon scattering at the interface and therefore, all samples satisfy the assumptions of the DMM or (ii) the interface disorder in all samples is weak and the transmission coefficient is always close to unity. Lacking a more quantitative theory of thermal conductance, we cannot at this time distinguish between these two limits.

ACKNOWLEDGMENTS

We thank S. Kodambaka for ellipsometry measurements of TiN and H. Maris for helpful discussions of experimental methods. This work was supported by DOE Grant No. DEFG02-01ER45938 and NSF Grant No. CTS 99-78822. Sample characterization used the facilities of the Center for Microanalysis of Materials which is partially supported by the U.S. Dept. of Energy under Grant No. DEFG02-91-ER45439.

*Electronic address: rcostesc@uiuc.edu
†Electronic address: d-cahill@uiuc.edu

[1] K. E. Goodson and Y. S. Ju, Annu. Rev. Mater. Sci. **29**, 261 (1999).
[2] C.-W. Nan, R. Birringer, D. R. Clarke, and H. Gleiter, J. Appl. Phys. **81**, 6692 (1997).
[3] G. Chen, *Phonon Transport in Low-dimensional Structures*, Vol. 71 of *Semiconductors and Semimetals* (Academic Press, San Diego, 2001), Chap. 5, pp. 203–260.
[4] D. G. Cahill, A. Bullen, and S.-M. Lee, High Temp.-High Press. **32**, 135 (2000).
[5] G. Soyez, J. A. Eastman, L. J. Thompson, G.-R. Bai, P. M. Baldo, A. W. McCormick, R. J. DiMelfi, A. A. Elmustafa, M. F. Tambwe, and D. S. Stone, Appl. Phys. Lett. **77**, 1155 (2000).
[6] D. A. Young and H. J. Maris, Phys. Rev. B **40**, 3685 (1989).
[7] E. T. Swartz and R. O. Pohl, Rev. Mod. Phys. **61**, 605 (1989).
[8] E. T. Swartz and R. O. Pohl, Appl. Phys. Lett. **51**, 2200 (1987).
[9] R. J. Stoner and H. J. Maris, Phys. Rev. B **48**, 16 373 (1993).
[10] A. Maiti, G. D. Mahan, and S. T. Pantelides, Solid State Commun. **102**, 517 (1997).
[11] A. V. Sergeev, Phys. Rev. B **58**, R10 199 (1998).
[12] D. Kechrakos, J. Phys.: Condens. Matter **3**, 1443 (1991).
[13] H. M. Streib and G. Mahler, Z. Phys. B **65**, 483 (1987).
[14] B. W. Karr, D. G. Cahill, I. Petrov, and J. E. Greene, Phys. Rev. B **61**, 16 137 (2000).
[15] C. A. Paddock and G. L. Eesley, J. Appl. Phys. **60**, 285 (1986).
[16] D. A. Young, C. Thomsen, H. T. Grahn, H. J. Maris, and J. Tauc, in *Phonon Scattering in Condensed Matter*, edited by A. C. Anderson and J. P. Wolfe (Springer, Berlin, 1986), p. 49.
[17] D. G. Cahill, K. E. Goodson, and A. Majumdar, J. Heat Transfer **124**, 223 (2002).
[18] K. E. O'Hara, X.-Y. Hu, and D. G. Cahill, J. Appl. Phys. **90**, 4852 (2001).
[19] W. S. Capinski, H. J. Maris, T. Ruf, M. Cardona, K. Ploog, and D. S. Katzer, Phys. Rev. B **59**, 8105 (1999).
[20] H. S. Carslaw and J. C. Jaeger, *Conduction of Heat in Solids* (Oxford University Press, New York, 1959), pp. 109–112.
[21] P. Flubacher, A. J. Leadbetter, and J. A. Morrison, Philos. Mag. **4**, 273 (1959).
[22] C. H. Shomate, J. Am. Chem. Soc. **68**, 310 (1946).
[23] R. Wietzel, Z. Anorg. Chem. **116**, 71 (1921).
[24] G. S. Parks and K. K. Kelley, J. Phys. Chem. **30**, 47 (1926).
[25] S.-M. Lee and D. G. Cahill, J. Appl. Phys. **81**, 2590 (1997).
[26] D. G. Cahill, S.-M. Lee, and T. I. Selinder, J. Appl. Phys. **83**, 5783 (1998).
[27] D. G. Cahill, Rev. Sci. Instrum. **61**, 802 (1990).
[28] J. O. Kim, J. D. Achenbach, P. B. Mirkarimi, and S. A. Barnett, Phys. Rev. B **48**, 1726 (1993).
[29] M. A. Durand, Phys. Rev. **50**, 449 (1936).